Intercomparison study and optical asphericity measurements of small ice particles in the CERN CLOUD experiment

Leonid Nichman[1,*,**], Emma Järvinen[2], James Dorsey[1, 3], Paul Connolly[1], Jonathan Duplissy[4], Claudia Fuchs[5], Karoliina Ignatius[6], Kamalika Sengupta[7], Frank Stratmann[6], Ottmar Möhler[2], Martin Schnaiter[2] and Martin Gallagher[1]

[1]{School of Earth, Atmospheric and Environmental Sciences, University of Manchester, Manchester M13 9PL, UK}
[2]{Institute of Meteorology and Climate Research, Karlsruhe Institute of Technology, Postfach 3640, 76021, Germany}
[3]{National Centre for Atmospheric Science, Manchester, UK}
[4]{Department of Physics, P.O. Box 64, 00014 University of Helsinki, Helsinki, Finland}
[5]{Laboratory of Atmospheric Chemistry, Paul Scherrer Institute, Villigen, Switzerland}
[6]{Leibniz Institute for Tropospheric Research (TROPOS), 04318 Leipzig, Germany}
[7]{University of Leeds, School of Earth and Environment, LS2-9JT Leeds, UK}
[*] {Department of Chemistry, Boston College, Chestnut Hill, MA, United States}
[**] {Aerodyne Research, Inc, Billerica, MA, United States}

Correspondence to: Leonid Nichman (Leonid.Nichman@manchester.ac.uk)

Abstract. Optical probes are frequently used for the detection of microphysical cloud particle properties such as liquid and ice phase, size and morphology. These properties can eventually influence the angular light scattering properties of cirrus clouds as well as the growth and accretion mechanisms of single cloud particles. In this study we compare four commonly used optical probes to examine their response to small cloud particles of different phase and asphericity. Cloud simulation experiments were conducted at the Cosmics-Leaving-OUtdoor-Droplets (CLOUD) chamber at European Organisation for Nuclear Research (CERN). The chamber was operated in a series of multi-step adiabatic expansions to produce growth and sublimation of ice particles at super- and sub-saturated ice conditions and for initial temperatures of –30, –40 and −50 °C. The experiments were performed for ice cloud formation via homogeneous ice nucleation. We report ~~the microphysical properties~~optical observations of small ~~quasi-spherical~~ ice particles in deep convection simulations and ~~small hexagonal ice particles typical for~~ in situ cirrus. Ice crystal asphericity and a degree of submicron complexity deduced from measurements of spatially resolved single particle light scattering patterns by the Particle Phase Discriminator mark 2 (PPD-2K, Karlsruhe edition) were compared with Cloud and Aerosol Spectrometer with Polarisation (CASPOL) measurements and image ~~s~~roundness captured by the 3View Cloud Particle Imager (3V-CPI). Averaged path light scattering properties of the simulated ice clouds were measured using the Scattering-Intensity-Measurements-for-the-Optical-detectioN-of-icE (SIMONE) and single particle scattering properties were measured by the CASPOL.

We show the ambiguity of several optical measurements in ice fraction determination of homogeneously frozen ice, in the case where sublimating quasi-spherical ice particles are present. Moreover, most of the instruments have shown a rather low sensitivity to the crystal complexity for small ice cloud particles that were grown under typical atmospheric conditions. Bulk averaged path depolarisation measurements of these clouds showed higher correlation to single particle measurements at high concentration and small diameters of cloud particles. These

results have implications for the interpretation of atmospheric measurements and parametrisations for modelling, particularly for low particle number concentration clouds. ~~This~~ The ensemble of optical instruments, ~~using~~ including both averaged path and single particle detection presented here, in conjugation with the CLOUD chamber, reveals the possible discrepancies in comparison~~s~~ of airborne and remote sensing measurements in different types of clouds.

1 Introduction

One of the first attempts to distinguish ice particles from water drops in the atmosphere was made almost 70 years ago in the Thunderstorm project (Byers and Braham,1948) during which it was noted that ice particles produce different sound than water drops when they impact the canopy of the aircraft. Since then, there have been many developments of airborne instruments for the measurement of cloud microphysical properties. Wendisch and Brenguier (2013) compiled a comprehensive list covering 48 different instruments, many of which are historical, but recently there have been several new developments, e.g. Abdelmonem et al. (2016) and Baumgardner et al. (2014). Many of the current techniques however are technological improvements on previous instruments originally developed and flown in the 1970's. An ongoing problem is the in situ measurement of concentrations of small ice crystals < 100 μm in size. Accurate measurements of ice crystal size distributions are necessary for evaluation of ice cloud radiative effects, development and evaluation of remote-sensing algorithms, evaluation of aerosol impacts, and ultimately correct representation of ice clouds in climate models (Jensen et al., 2009).

This microphysical information is also important in research of early ice formation when initial ice particles in low concentrations push the sampling volume limits of many instruments (Johnson et al. 2014). Optical methods are preferably employed both for remote sensing of clouds and for in situ single particle measurements. For the detection of particle shape and structure, the scattering intensity of single particles is ~~most~~ commonly used. This technique is compared here with the mean scattering intensity from ensemble measurements, where shape information is averaged due to different orientations of the particles in the measuring volume (Sachweh et al. 1999).

Droplet concentration in clouds normally varies between several tens to hundreds cm^{-3} while typical ice crystals concentration is normally a few particles L^{-1} but can reach ~100 L^{-1} in old clouds (Wallace and Hobbs, 2006). The diameter of single droplet or ice crystal is normally in the super-micron range and can reach several hundred μm. The initial shape of ice particles may be indistinguishable from water droplets. Optically ambiguous shapes of liquid and solid cloud particles such as water, frozen droplets and quasi-spherical ice (Gayet et al., 2012; Järvinen et al., 2016c) may be detected simultaneously in the troposphere. Some of these particle phases coexist for long periods of time e.g. in long-lived mixed-phase stratiform layers (Korolev and Isaac, 2003a). The resolution of most optical probes, coupled with coincidence problems, prevents a clear determination of particle shape for particle sizes smaller than 100 μm in such clouds. In glaciated clouds, Cober et al., (2001) applied geometric formulas to 2D images, identifying between 5 and 40 % of them as circular. Spherical particles were observed in large numbers by Korolev and Isaac (2003b) even in clouds sub-saturated with respect to water. Moreover, Lawson et al., (2006a) reported that particles < 50 μm account for 99 % of the total number concentration, 69 % of the shortwave extinction, and 40 % of the mass in mid-latitude cirrus.

however, these measurements were contaminated with particle shattering. As a result of this shape ambiguity and low resolution of small sizes, our fundamental knowledge of small cloud particle microphysics is far from being complete.

Large super-cooled water droplets up to 5 mm in diameter exist only at warmer ambient temperatures, but smaller cloud droplets may frequently exist in a super-cooled state down to –20 °C, and less frequently as low as the homogeneous freezing level (Elliott and Smith, 2015; Rosenfeld and Woodley, 2000). Furthermore, very small super-cooled water droplets may stay in a metastable liquid condition down to –40 °C (Korolev et al., 2003a). Pilots often reported deviating around convective clouds due to the danger of ice accretion of super-cooled droplets (Jeanne et al., 2006). Therefore, an inaccurate classification of spherical shapes may directly affect the routes and costs of commercial flights (Gallagher et al., 2016).

Frozen droplets are an important feature of mid latitude anvil cirrus. In fact, frozen droplets and frozen droplet agglomerates are a dominant particle type also in higher anvil outflow clouds (Stith et al., 2014; Järvinen et al., 2016c). Frozen droplets could also be responsible for first ice initiation in deep convective clouds (Taylor et al., 2016). Although frozen droplets are frequently measured, our understanding of the microphysical and optical properties of these quasi-spherical ice particles is somewhat vague. The process by which frozen droplets are formed can play an important role in their morphology. Microscopic structures, like surface roughness, as well as detailed information on the aspect ratios of the frozen droplets found in clouds are key variables required to determine the optical parameters that are included in the modelling and prediction of the climate effect of these cloud systems.

In addition, quasi-spherical ice shapes are common in cirrus. Luebke et al. (2016), Garrett et al., (2005) report the presence of many quasi-spherical ice particles in cirrus, especially at the smaller sizes. Quasi-spherical ice prevails also in contrails at low temperatures below about –55 °C. In the core of the contrail, high crystal concentrations reduce the vapour density to saturation causing the ice particle to retain a nearly spherical shape (Lawson et al., 1998; Lynch, 2001). Contrail cirrus cover is small compared to natural cirrus; nonetheless, they still have a climatic impact with the constant increase in jet aircraft traffic (Stordal et al., 2005; Irvine and Shine, 2015).

Cloud particles measurements on aircraft campaigns inherently suffer from limited spatial coverage and limited instrument sampling volumes. Cirrus clouds do not have an obvious formation stage, and therefore it is not possible to reliably position a research aircraft in their development stage (Lawson et al., 2006a). Remote sensing provides averaged features but is insensitive in cases of subvisual or contrail cirrus. Conversely, chamber experiments provide a well-controlled and pristine environment for simulations and instrumental comparison, although the role of the ice nucleation process in the atmosphere may change with time through the life cycle of a convective cloud for example, and is strongly influenced by the environmental airflow (Heymsfield et al., 2005).

Our chamber campaign investigating the homogeneous freezing process relevant to the upper region of deep convective clouds and in situ formed cirrus in pristine environments was conducted at the European Organisation for Nuclear Research (CERN) in 2013, hereafter referred to as CLOUD 8. The goal of the experiments presented here was to complement and extend the results previously obtained in the Aerosol Interaction and Dynamics in the Atmosphere (AIDA) chamber with similar instruments (Järvinen et al., 2016c; Schnaiter et al., 2016) such as observation of morphological features and confirmation of a possible pathway for

quasi-spherical ice formation which affects growth and sedimentation mechanisms of ice in clouds. Additionally, a comparative analysis of four optical probes is reported in this paper to provide clarification of optical measurements in several respects: single particle versus averaged path optical measurements, polarisation measurements versus depolarisation and asphericity derivation i.e. using scattering patterns of the near-forward scattered light in the Particle Phase Discriminator mark 2 (PPD-2K, Karlsruhe edition), single particle polarisation properties in the Cloud and Aerosol Spectrometer with Polarisation (CASPOL), and image analysis in the 3View Cloud Particle Imager (3V-CPI). ~~We then use the a~~Asphericity is often used to determine the ice fraction in a cloud by prescribing an aspherical shape for all the ice particles, and hence assum~~e~~inge that ice fraction is equivalent to an aspherical fraction, this practice is tested in our experiments.

2 Methodology

2.1 The CLOUD chamber

The chamber facility at CERN is described in detail by Duplissy et al. (2016), Kirkby et al., (2011) and Guida et al., (2013). The expansion system installed at the Cosmics Leaving OUtdoor Droplets (CLOUD) chamber allows production of relatively high cooling rates, above 5 °C min^{-1}, compared to the AIDA chamber, where maximum cooling rate of 4 °C min^{-1} is typically achieved (Möhler et al. 2006; Järvinen et al., 2016c). Stronger cooling rates will activate a higher fraction of the aerosol by driving higher peak super-saturation. Since the liquid water content that freezes does not vary with updraft strength, the freezing of more numerous droplets in the faster updrafts simply produces smaller ice particles. This is clearly shown by Ackerman et al. (2015) where ice particle mass distributions in homogeneous freezing for stronger updrafts produce substantially smaller ice particles ~~and greater ice water content~~. Schnaiter et al. (2016) further showed that high ice particle growth rates also enhance the formation of small-scale complexity, such as ice particle surface roughness. Gayet et al., (2011) reported that in a deeply rough surface the mean free path length between two subsequent inclusions was equal to 15% of the diameter of the circle circumscribing the hexagonal facet of an ice crystal. Following the procedure suggested by Schnaiter et al. (2016), we have simulated similar conditions for the derivation of aspherical fractions and instrumental inter-comparison in the CLOUD chamber (Fig. S1), where ice particles are sequentially sublimated and then grown under different supersaturated conditions. The multistep adiabatic expansion mechanism has allowed the regrowth of ice after sublimation as will be explained in the next section.

2.2 Overview of the homogeneous freezing experiments

In the cloud chamber experiments, we have simulated some of the homogeneous freezing processes taking place in the deep convective cloud systems i.e. with updraft velocities up to 5 m s^{-1} with corresponding cooling rates up to 5.8 °C min^{-1}. In the following sections we present the evolution of the ice particle shape and small-scale complexity upon freezing, sublimation and re-growth periods from selected representative individual experimental runs. Overall, all the results from repeated individual experiments agreed well with each other. A representative list of the conducted experiments can be found in Table 1. The technical description of the CLOUD chamber pressurisation, CCN injection and expansion of the air volume in a multi-step regime is given in detail elsewhere (Nichman et al., 2016; Duplissy et. al., 2016; Guida et al., 2012, 2013) and will be briefly described here.

Continuous attempts to find an accurate cloud classification have led to suggestion of new definitions of liquid origin clouds and in situ cirrus (Krämer et al., 2016; Luebke et al., 2016). Liquid origin cirrus class comprises of ice crystals formed by homogeneous freezing of liquid drops farther below in the atmosphere which are uplifted into the cirrus temperature range. In situ cirrus class cloud may form in fast updraft triggered by jet streams or lee waves. This class has high IWC and many, small ice crystals. The formation mechanism in this case is insensitive to IN properties and dominated by homogeneous freezing. Our expansion profiles allow simulation of both types of clouds.

The homogeneous freezing experiments were started in a pressurized chamber volume, at 123.3 kPa, with a CCN injection. The sulphuric acid solution droplets, used as CCN, were generated in a sulphuric acid generator consisting of heated sulphuric acid reservoir and airflow past the reservoir. A more detailed explanation of the generation method can be found in Wagner et al. (2008). By varying the duration of the sulphuric acid injection, we controlled the number concentration of the sulphuric acid droplets, and by adjusting the temperature of the sulphuric acid reservoir and the airflow rate through the heated reservoir we controlled the mean size of the aerosol particles.

The chamber is surrounded by an insulated thermal housing which allows a precise regulation of the temperature with stability within 0.1 °C. The in situ temperature values are measured close to the centre of the chamber, at 1.2 m distance from the walls using a PT100 temperature sensor (Duplissy et al., 2016; Dias et al., 2016). For pressure monitoring in the chamber, we used the VEGABAR 53 process pressure transmitter, VEGA. The total humidity inside the chamber was measured by a fast chilled-mirror frost-point hygrometer (MBW, model 373LX). The supersaturations with respect to water and ice (Fig. 1a) were calculated from dew and frost points using water and ice saturation vapour pressure at the measured temperature (Buck, 1996) with deduction of the contribution from the condensed phase due to a higher temperature in the MBW sampling line.

At the beginning of most experiments, we generated low concentrations (~ 100 cm^{-3}) of sulphuric acid aerosol counted with a condensation particle counter (CPC, TSI model 3010). At these concentrations, all seed aerosols will act as CCN at almost the same time and further homogeneous nucleation and growth of the ice crystals would occur upon further expansion cooling. All the experiments were initiated slightly below ice saturated conditions at temperatures near –30, –40 and –50 °C (Figs. 1a, A1). In the experiments starting at –30 °C we cooled the chamber air by expanding the volume until super cooled liquid droplets were formed. The droplets were grown by further cooling until ice started to form by homogeneous freezing of the super-cooled water droplets. The ice particles then grew until the expansion was stopped and the formed ice crystals started to sublimate under ice sub-saturated conditions, induced by an increase of temperature due to the heat flow from the warm chamber walls. A second step in the expansion profile allowed the regrowth of the sublimating particles. The experiments at ~~–40 and~~ –50 °C were started similarly by cooling the chamber volume until the first ice particles were formed by deposition nucleation. After the first ice particles were detected and had grown in diameter (Table 1), we proceeded to the next step of the multistep expansion profile as discussed above.

2.3 Cloud probes

2.3.1 PPD-2K

The light source in the PPD-2K instrument is a frequency doubled Nd:YAG laser which emits 100 mW at a wavelength of 532 nm. The sensitive areas of the trigger detector and camera are identical (~2.5 mm^2). The

classification of cloud particles by the PPD-2K is based on a spatial analysis of high resolution intensity patterns of single particles in the 5 to 26° forward angular range. In the scattering patterns of (spherical) droplets we normally observe concentric rings at angular positions corresponding to the maxima intensities given by Mie-theory. The sampling flow of the instrument was set to 5 lpm with a sheath flow of 2 lpm. Although we know that diffraction instruments (e.g. SID-1, SID-2, SID-3, Hirst et al., 2001; Cotton et al., 2010; Vochezer et al., 2016) suffer from major coincidence errors at high concentration and mixed phase clouds, in these chamber experiments ~~we did not observe coincidence errors~~the probability for coincidence was negligible, lower than 1% in most cases.

We used computerised discrimination of images with concentric rings from images without the rings based on variance calculation of the image pixels along the polar integrated azimuthal intensity profiles (Vochezer et al., 2016; Järvinen et al., 2016c). Aspherical fractions were determined by applying a threshold variance value of 10^{-5}. This threshold is used based on the visual inspection of diffraction patterns of ice and droplets in chamber experiments. Images with low variance corresponded to concentric rings and were classified as spherical (e.g. droplets). Similarly, in the case of ice particles with mean variance below this value the particles were classified as spherical. Ice habits e.g. columns and plates have characteristic scattering patterns which allow classification of the detected particles. More technical details are described in Vochezer et al. (2016).

2.3.2 SIMONE

The averaged path SIMONE-Junior (Järvinen et al., 2016b), was installed in the chamber for bulk depolarisation measurements. This instrument is comparable to a lidar and is used to detect phase-transitions in aerosol, cloud particle ensembles, and to investigate the microphysical properties of clouds. The instrument projects a 552 nm polarised (e.g. perpendicular, parallel and circular) light beam and detects from a volume of a few cubic centimetres. Unlike a lidar measurement, parallel and perpendicular components of the backscattered light are measured around the detection angle of 176°, at a very confined angular range with an acceptance angle less than 0.8 mrad. The linear depolarisation ratio is zero for spherical particles and non-zero if particles' shape deviates from a sphere, thus a detection of the bulk cloud phase is possible. Forward scattering intensity is measured at 4°. The operation of the SIMONE in the CLOUD chamber is described in detail by Järvinen et al. (2016a). The basic instrument concept and data interpretation in case of chamber ice clouds is detailed in Schnaiter et al. (2012).

2.3.3 Airborne probes

CASPOL

The CASPOL installed in the chamber was part of the Cloud, Aerosol, and Precipitation Spectrometer (CAPS, Droplet Measurement Technologies), an instrument commonly used on aircraft for cloud microphysical measurements (e.g. Baumgardner et al., 2001; Johnson et al., 2012; Luebke et al., 2016). The CASPOL relies on incident laser-scattering by single particles. The version of CASPOL employed here has a linearly polarised laser to provide a collimated incident beam of light at a wavelength of 680 nm and a sample area of ~0.225 mm^2. The collecting optics guide the light scattered in the 4 to 12° subtended cone into a forward-sizing photodetector. This light is measured and used to infer particle size. However, the CASPOL is calibrated with spheres and aspherical particles are mis-sized (Borrmann et al., 2000). We estimate the sizing error would normally be of the order of the size bin width.

The backscatter detector measures the scattered light cone subtended by the angles 168 to 176°. Additionally, this version of CASPOL measures the polarised fraction of the backscattered light in the orthogonal plane for the first 292 particles s^{-1} (Droplet Measurement Technologies Manual, 2011). This functionality allows discrimination of aspherical particles in the 0.51 - 50 µm range. For spherical particles, typically droplets, the polarisation of the incident light will be preserved and the orthogonal polarisation in the back-scatter will generate nearly zero signal. Depending on the asphericity of the particles, there will be increased signal in the backscatter polarised detector. An increase in size with decrease in polarisation in CASPOL at temperatures below the frost point will mean that ice is sublimating and becoming more spherical (Jensen et al., 2010). The classification of droplets and ice in CASPOL data analysis is primarily based on polarisation threshold which needs to be determined from laboratory experiments (Nichman et al., 2016). The sampling air speed of the instrument was ~4 m s^{-1}. Highest particle arrival rate was 500 s^{-1} while the average rate was below 100 s^{-1}.

3VCPI

Another aircraft mounted instrument is the Cloud Particle Imager which can image and count particles in the size range of 15–2500 µm, with the images having a nominal 2.3 µm resolution. The newer 3V-CPI (SPEC Inc.) is essentially a 400 frame per second CPI probe (Lawson et al., 2001) integrated with a 2D-S probe (Lawson et al., 2006c). The particle detection system consists of two intersecting elliptical cross section continuous laser beams (30 mW, 788 nm). For detection, a particle must scatter light from both beams. This in turn triggers the imaging laser (pulsed 80 W, 850 nm), which fires onto a CCD camera. CPI obtained information covers particle size (including area and volume) and ice habit classification (Lawson et al., 2006b; Um and McFarquhar, 2009; Lindqvist et al., 2012)~~Heymsfield et al., 2010)~~. Complementary size distributions and concentrations data are obtained by the 2D-S. The 3V-CPI is especially suitable for use in ice and mixed phase clouds (~~Lawson et al., 2003;~~ Gayet et al., 2012; Stith et al., 2014). Each of the 2.3 µm resolved surface images captured by the CPI can be fitted to a circle function to determine the roundness of the particle (Korolev and Isaac, 2003b). Temporal changes of roundness can be used to calculate the mean non-round (aspherical) concentration fraction. However, the roundness parameter for smallest detected particles of 10 µm optical diameter, have the largest uncertainty as will be discussed in Sect. 3.2.

The 3V-CPI was mounted on top of the chamber for vertical sampling of larger cloud particles to reduce sedimentation in the sampling lines. The outlet of the instrument was connected to vacuum line and sample air speed of ~4 m s^{-1} was maintained.

3 Results and discussion

3.1 Experimental description

3.1.1 Ice nucleation and regrowth

The air pressure and mean temperature profiles for a typical expansion procedure in accordance with Schnaiter et al. (2016) are presented in Fig. 1a. The expansion starts first with a slow pressure decrease to create water-supersaturated conditions inside the chamber and to form a cloud of super-cooled droplets. The expansion rate is increased towards the end in order to achieve ice-supersaturated conditions in a short time period and to nucleate the ice almost simultaneously. The overall cooling rate during this expansion was –4.9 °C min^{-1}. The PPD-2K

measured the size distribution during the expansion (Fig. 1b). The cloud period with super-cooled droplets lasts only a few seconds and followed by almost immediate and fast ice formation. The depolarisation signal measured by the SIMONE increases promptly after the increase in the forward scattering signal indicating the short droplet period followed by the fast formation of ice (Fig 1c). The expansion is then stopped at ~ 1 min (Fig. 1a).

After the first step of the expansion, the initial temperature of the air volume is slowly restored by the heat flux from the warmer chamber walls, thus creating sub-saturated conditions inside the chamber. This warming leads to the sublimation of ice crystals and the observed changes in their microphysical properties. A re-growth of the sublimating ice crystals is initiated at ~ 11 min, when the pressure decreases from 111.3 to 101.8 kPa. The depolarisation signal increases once again during this step and reaches slightly higher levels (0.34) than in the first step (0.26), together with an increasing noise level due to the low number concentration. There is also a small increase in the forward scattering but this is much lower than in the first step of the expansion due to ~5 fold decrease in the concentration. We assume a complete glaciation in the first step without any significant reactivation in the number concentration during the regrowth period (Fig 1c).

3.1.2 Size range overlap

In this comparison, the overlapping size range of PPD-2K and CASPOL for measurements of small ice particles is 7 – 50 μm (Fig. 1b). However, only 41 % of the particle-by-particle (PBP) polarisation data in CASPOL at –30 °C were from particles larger than 7 μm. At lower temperatures the particle size distribution (PSD) is shifted towards the grey area in Fig. 2, below the PPD-2K size cut-off. The fraction of CASPOL PBP polarisation data points from particles > 7 μm at lower temperatures was even lower: 24 % (–40 °C), 32 % (–50 °C), thus, most of the particles in the cloud that produce the polarisation data in the CASPOL are small, < 7 μm, while in the PPD-2K data 100% of the analysed particles are > 7 μm.

The size segregated aspherical fractions as measured by the PPD-2K in the overlapped size region are presented in Fig. 3. At –30 °C, the large ice particles reach 20 μm in diameter during the first step of the expansion and grow up to 35 μm during the second step, within the detection range of CASPOL. Ice particles formed under different temperature regimes would have a different morphology. At cirrus temperatures below –40 °C, the ice particles form directly from the vapour phase via deposition nucleation (Figs. 3b, 3c), a different formation pathway compared to ice formation through the liquid phase at –30 °C (Fig. 3a). At the final step of the expansion at –30 °C, during the sublimation period, the aspherical fraction is extremely low due to sphericity ambiguity as will be discussed in Sect. 3.3. For better statistical characterisation we achieved longer cloud life time at lower temperatures, up to 45 min. However the measurements of PPD-2K at these temperatures were somewhat incomplete, missing the smaller sizes and hence the initial steps of cloud particle formation and growth especially during the first step of the expansion (Figs. 3b, 3c). The temperature~~s~~ and supersaturation profiles of runs: 1276.05 (–40 °C), and 1298.12 (–50 °C) are shown in Fig. A1~~S1~~.

3.1.3 Column fraction

The ice fraction contains ice habits such as plates and columns in all the regrowth experiments discussed here (Table 1). The largest fraction detected by PPD-2K at different temperatures was composed of ice columns as shown in Fig. 4. In the first part of experiment 1292.01 (–30 °C) the frozen droplets are grown at lower

temperature and higher super-saturation than in the second sublimation period of this experiment (Fig. 1a), leading to a formation of complex particles (Sect. 3.3). In the regrowth period, the temperature drop and super-saturation conditions are more moderate and we observe the formation of columnar ice particles. The columnar shape is not preserved and the ice particles sublimate to their underlying spherical core as seen in Fig. 3a. The largest column fractions were measured at the lowest temperature –50 °C (Fig. 4c). ~~Although we know that diffraction instruments (e.g. SID-1, SID-2, SID-3, Hirst et al., 2001; Cotton et al., 2010; Vochezer et al., 2016) suffer from major coincidence errors at high concentration and mixed phase clouds, in these chamber experiments we did not observe coincidence errors.~~

3.2 3V-CPI image analysis of ice particles

High concentrations of particles grew above 20 µm in diameter (Fig. 1b), thus allowing their detection with the 3V-CPI instrument. Quasi-spherical or quasi-spheroidal small particles were identified from the CPI images (Fig. 5). The CPI imager is triggered by the 2D-S component for particles larger or equal to 10 µm as described in Sect. 2.3.3. The image analysis can provide the roundness of the particles. Due to the larger error in small sizes, Korolev and Isaac (2003b) have considered the roundness of the particles with diameter larger than 20 µm is appropriate. Connolly et al. (2007) have included the roundness of smaller particles of 10 µm in diameter in their analysis using size and shape corrections based on tests with ice analogues to the instrument's depth of field. Emersic et al. (2015) chose a roundness threshold of 0.9 for phase discrimination of particles larger than 35 µm. The exact definition and calculations of roundness are described in detail in the papers above. In this analysis we consider particles in the range of 20–50 µm for broader coverage of the CASPOL and PPD-2K size ranges while constraining the uncertainty in the roundness parameter. Here, the threshold for phase discrimination by roundness was set to 0.9.

Analysis of a large dataset of CPI images by Korolev et al., (2003c) showed that in glaciated clouds a large fraction of particles with diameter < 60 µm do indeed have a quasi-spherical compact shape. Korolev and Isaac, (2003b) noted that the question of spherical ambiguity remains due to optical limitations of the instruments. Despite the limitations of size range and resolution, Fig. 6a shows an increase of the non-round image fraction during the growth periods of the ice particles in our chamber experiments.

3.3 Aspherical fractions measured by PPD-2K, CASPOL, 3V-CPI

In airborne measurements, ice fractions are commonly derived from the optical asphericity of the particles (Sect. 1). Here we compare PPD-2K and CASPOL single particle measurements to examine their ability to distinguish between droplets and ice particles in different ice nucleation modes. In experiment no. 1292.01 (–30 °C), all the droplets freeze simultaneously, almost immediately after their formation, concluding the duration of the pure liquid cloud in the order of seconds (Fig. 6a). Promptly after freezing we measure a high ice (aspherical) fraction (~100 %), as expected. The freezing onset is detected by the increase in the depolarisation signal from the SIMONE, and proceeds with an increase in 3V-CPI smoothed- non-round fraction (Sect. 3.2) annotated by pink markers, both indicating the presence of non-spherical particles. In the sublimation period, at 4 min, we see the reversed transition in the aspherical fraction; we start to detect more spherical particles that are classified as liquid droplets according to the thresholds used to classify ice (Sect. 2.3; Nichman et al., (2016)). The depolarisation finally decreases (Fig. 6a), and particles are no longer detected by the 3V-CPI due to their

decrease in size below the threshold. The size segregated aspherical fraction measured by the PPD-2K for this experiment is shown in Fig. 3a.

During the sublimation periods the aspherical fraction decreases implying increasing sphericity of the particles (Fig. 6a). However, once full glaciation was observed, the liquid phase cannot subsequently exist at the ambient chamber temperature; below –30 °C. Therefore, the nearly spherical particles observed (4–10 min and from 19 min onwards) are spherical ice and not liquid water droplets. In atmospheric measurements, such an aspherical fraction would normally be converted into an ice fraction. In this cloud simulation, at the end of the sublimation period, both instruments misinterpret the total ice fraction as spherical-liquid by 60%.

In experiments 1276.05 (–40 °C) and 1298.12 (–50 °C) (Figs. ~~5b~~6b, ~~5c~~6c), we observe a short increase of aspherical fraction measured by the 3V-CPI at –40 °C and insufficient data in this size range at –50 °C. A~~a~~ lower aspherical fraction is measured by the CASPOL at ~~a lower~~ these temperatures. Polarisation data analysis therefore suggests that ice particles smaller than 7 µm are more spherical at lower temperatures (Fig. 6c red line) and they are more abundant (Sect. 3.1.2). Furthermore, the aspherical fraction for all particles detected in the PBP mode in CASPOL at –50 °C follows the SIMONE depolarisation time series while the aspherical fraction of CASPOL >7 µm subgroup is higher and increases towards the end of the expansion (Fig. 6c). The size dependence of these two polarisation detection techniques is demonstrated in Sect. 3.4. However, scattering patterns detected by the PPD-2K showed a 100% aspherical fraction in both experiments with vapour formed ice crystals. Additional studies are required to confirm these trends.

Similar discrepancies in aspherical fraction measurements by PPD-2K and CASPOL were shown already by Järvinen et al., (2016c) for ice particles formed via homogeneous nucleation and via deposition nucleation on mineral dust at –30 °C. The asphericity of the particles significantly differs for ice formed through the liquid phase and ice formed through the vapour phase. These discrepancies (Figs. 5b, 5c) at lower temperatures can be partially explained by the decrease in the number of particles measured in every second and therefore large standard deviation in aspherical fraction calculation i.e. 19 % for particles > 7 µm at –40 °C and 37 % for particles > 7 µm at –50 °C. However, the smaller size of particles at –40, –50 °C is the main cause of reduced sensitivity of the polarisation measurements with respect to aspherical features as will be explained in the next subsection.

The impact of small-scale surface complexity on phase discrimination

The resolution of instrumentation employed in atmospheric measurements, commonly, is not sensitive enough to image the surface microstructural features of the ice crystals. The resolution of the widely used CPI probe is around 2 µm, i.e. in the same range as the smallest droplets that are frozen into ice crystals and significantly larger than the size of the ice crystals' surface anomalies. Although these anomalies, like roughness and stepped hollowness of the crystal, do not significantly contribute to the mass distribution, they can significantly alter the light scattering properties of the ice crystals, as discussed in the introduction.

We have analysed the scattering patterns of the PPD-2K instrument to determine the surface features of individual ice crystals as described in detail in Schnaiter et al. (2016). This instrument is sensitive to features that are on the order of the wavelength used, 532 nm. The particle's surface complexity or non-uniformity manifests itself as speckles in the diffraction patterns (Järvinen et al., 2016c), where the analysis of spatial uniformity of the scattered light intensity with the Grey-level Co-Occurrence Matrix (Schnaiter et al., 2016)

indicates the small-scale complexity of an ice crystal. The so called k-value defined as a complexity parameter by Schnaiter et al. (2016) can reflect the physical complexity in a higher k-value. However we should emphasize that at present it is not possible to quantitatively relate this value to an actual degree of complexity or surface uniformity of the particle. We also note here that although a k-value can be calculated from the PPD-2K instrument, the k-value is not calibrated for this instrument. Therefore, in this study we can only conclude about the relative variations in this complexity parameter.

Figure 7a shows the size segregated k-value in experiment no. 1292.01. The experiment starts with a period of super cooled liquid droplets, where scattering patterns of concentric rings are observed (scattering pattern A in Fig. 7a). The freezing of the droplets takes place almost simultaneously and all the freshly frozen droplets exhibit surface features i.e. the PPD-2K scattering patterns are speckled without the normal concentric ring features (scattering pattern B in Fig. 7a). Seemingly the frozen droplets develop a frost layer (Järvinen 2016c) on their surfaces during the freezing and initial growth. However this layer was too thin to be detected by the other instruments.

During the sublimation period, the complexity of particles noticeably decreased (Fig. 7b). The smooth frozen droplets were found at smaller sizes compared to the frozen droplets with small-scale complexity. The sublimation of the frost can be seen in scattering patterns C and D (Fig. 7), where the diffraction pattern D cannot easily be distinguished anymore from that of a liquid droplet, i.e. the frozen droplet in question is almost a perfect sphere.

The re-growth of the sublimating frozen droplets, achieved by again starting expansion leading to ice super saturated conditions. The surface frost layer developed again immediately after super saturation is reached and the median complexity parameter reaches its highest value (Fig. 7b). Consequently, these particles are immediately classified as aspherical. The observed complexity of pattern B reappears on pattern E i.e. on the columns (Figs. 4a, 7). The re-grown ice crystals were again allowed to sublimate after the growth period. Similar smooth frozen droplets were detected as in the first sublimation period, together with a decline of the detected aspherical fraction.

The small-scale complexity significantly changes the scattering patterns measured by the PPD-2K (Fig. 7). Therefore, the observed speckled patterns can be easily classified as aspherical, which leads to a robust and high ice fraction, if complex ice particles are present. Sublimating columnar particles that demonstrate lower complexity (Fig. ~~S2~~A2) are classified as aspherical in the PPD-2K. Only optically spherical sublimating frozen droplets are misclassified as droplets by the automatic algorithm. However, with visual inspection it is still possible to discriminate between a smooth ice sphere and a spherical liquid droplet (compare patterns A and D in Fig. 7). However, other optical instruments (e.g. CASPOL) can misclassify complex ice particles if they are too small, and underestimate the aspherical fraction if their occurrence is low.

3.4 Single particle polarisation and ensemble depolarisation ratios

This analysis aimed at improving our interpretation of the small ice particle polarizability and the comparison of different instruments and their approaches to discriminate small liquid and ice phase cloud particles by properties of the scattered light. One such property is the linear depolarisation ratio for parallel incident laser polarisation $\delta_{||}$ which is defined as the perpendicularly polarised to parallel polarised ratio of the backscattered light intensity ($I_{\perp}/I_{||}$). This ratio is frequently used in remote sensing (e.g. Burton et al., 2012; Petzold et al.,

2010). The linear polarisation ratio in CASPOL data analysis is defined as the fraction of the perpendicularly polarised backscattered light from the total backscattered intensity (Dpol/Back) as previously reported (Glen and Brooks, 2013) and is used for ice fraction derivation (Nichman et al., 2016). The particle detection method and the measured polarisation components are not the only dissimilarities in these instruments, they also operate at different wavelengths, have slightly different collection angles and two orders of magnitude difference in the sample volume (see Sect. 2.3).

Depolarisation ratio measured by the SIMONE and the polarisation ratio measured by the CASPOL were plotted against each other with 1 s temporal resolution for run no. 1292.01 (high concentration and small diameter), no. 1291.12 (low concentrations and big diameter), no. 1291.07 (high concentration and small diameter) and no. 1298.2 (low concentration and small diameter) (Table 1) are shown in Fig. 8. The dimensions of the marker reflect the number concentration, with the highest at 56 cm^{-3}. The CASPOL polarisation ratios presented here are based on 1 s averages for all particles larger than 3 μm. Small aerosol particles (< 3 μm) were detected during background measurements; after CCN injection and before the expansion. These small particles i.e. non-activated aerosols were excluded from further analysis.

The lowest correlation was found at low concentration, where the detected polarisation is higher than the depolarisation. This is partially due to averaging deviation at low concentration within the large sample volume of the SIMONE instrument. Generally, we have observed higher correlation between the instruments in cases with high concentration and small diameters of cloud particles (R^2 ~ 0.35) (Fig. 8a, 8b) and almost no correlation (R^2 ~ 0.01) in cases with low concentrations and larger sizes of cloud particles.~~Nonetheless, in several cases a surprisingly reasonable correlation is observed (Fig. 8a, 8b). Generally, we have found that higher correlation is observed between the different instruments in cases with high concentration and small diameters of cloud particles (R^2 ~ 0.35). Low correlation (R^2 ~ 0.01) is observed in cases with low concentrations and larger sizes of cloud particles.~~

3.5 Implications for atmospheric measurements

The classification of quasi-spherical ice as liquid droplets is posing a problem in atmospheric measurement and especially in mixed-phase clouds, where the ice fraction calculations can be affected by the misinterpretation presented in this paper. In these chamber experiments, we know that all the particles in the sub-saturated conditions are in the ice phase, which allows us to use the spherical classification method to distinguish spherical ice particles in cold clouds. In the atmosphere, there are additional possible crystal rounding mechanisms e.g. equilibrium thermal roughening near 0 °C, a surface coating of solution, kinetic roughening at high super saturations, and latent heat-induced melting of the surface during growth at high temperatures and super saturation. In addition, frozen droplets retain their rounded appearance until sufficient growth occurs. Therefore, it is not possible to infer sub-saturated conditions in the atmosphere merely by sampling rounded crystals (Nelson 1998) and the measured ice fraction is prone to significant underestimation. In any case of small quasi-spherical particle~~s~~ detection at sub-zero temperatures in the atmosphere, we recommend to ~~compare the data of more than one instrument~~use multiple instruments for intercomparative analysis.

~~Ice~~ Aspherical fraction derived from CASPOL data can be compared to other instruments with higher confidence when the PSD is fully covered by the overlapped size and concentration range of the instruments with sufficient number of particles for ~~ice~~ aspherical fraction derivation and low standard deviation. Such a

comparison can reveal the true ice fraction. However, artefacts such as shattering, compression, and coincidence (Lance et al., 2012) that may occur in airborne measurement but do not occur in this setup may cause a mis-estimation of the ice fraction. In case small particle arrival rate and the concentration do not exceed the values reported here, the findings of this study may be applicable.~~However, high concentration may cause coincidence and misestimation of the ice fraction~~.

The comparison of remote sensing and PBP measurements is not a straightforward process (i.e. bulk vs. single particle and single complexity vs mixed-complexity ensembles of particles). Many single particle and ensemble measurements laboratory techniques in particular have proven difficult to adopt when translated to real atmospheric environments. These techniques often provide complementary data rather than comparable data (Lynch, 2001) and research in this area continues. Based on our analysis, ensemble depolarisation measurements of cloud particles at ~~certain~~ concentrations above 20 cm^{-3}, sizes below 15 µm and certain atmospheric conditions can be comparable to single particle polarisation airborne measurements.

Recent efforts to classify clouds (e.g. Krämer et al, 2016; Luebke et al, 2016) by their microphysical properties did not account for particle morphology in their study; the morphology of small ice of in situ cirrus or of liquid origin clouds in the first steps of homogeneous freezing may affect the scattering properties and hence the solar radiation budget. According to the findings in this paper, the complexity might be present however undetectable by some instruments at lower temperatures or small sizes (<7 µm). It may increase scattering and thus intensify cooling while the lack of complexity of liquid origin clouds in warmer subzero temperature may allow more efficient warming. However, this should be further investigated.

4 Conclusions

We have presented an instrumental setup for combined single cloud particle and ensemble measurements for assessment of the relative optical ice and liquid responses in each case. The results were used to determine the ~~ice shape~~asphericity and small-scale complexity evolution during adiabatic expansion, sublimation and regrowth as well as for potential impact on phase discrimination. We report observations of super-cooled and frozen droplets, small ice habits and spheroids in a series of CLOUD chamber experiments at –30, –40 and –50 °C.

We have shown that the small quasi-spherical ice particles produced in the sublimation process exhibit a similar optical behaviour to that of water droplets in the PPD-2K variance analysis and in the CASPOL polarisation analysis for high PSD overlap at –30 °C. The analysis of the scattering patterns shows the similarity of the spherical states and the difficulty in applying automatic phase discrimination. Therefore, observations of small spheroids (< ~~60~~ 40 µm) in sub-saturated conditions might be highly ambiguous. These results indicate that small quasi-spherical ice misclassification might similarly concern numerous optical instruments, impactors and other probes that were not examined here. Nonetheless, the scattering patterns differ for quasi-spherical ice and water due to small deviations from sphericity. An increase of resolution in future versions of the optical instruments might amplify this discrimination and reveal additional subtle features. In atmospheric measurements, small particle detection is often contaminated by shattering therefore coincidence should be addressed before any comparison can be made.

We have shown a chamber simulation of small-scale complexity evolution on a frozen droplet during an updraft and in sub-saturated conditions. In regions with high concentration of small cloud particles (< ~~60~~ 40 µm), the

observed differences in morphology will affect the observed radiative properties, growth mechanisms, aggregation and charging in clouds. The aspherical fraction detected by the PPD-2K could be described with a high degree of small-scale complexity which was undetectable by the other instruments. ~~This complexity measurement can be potentially calibrated in future experiments to derive the complex fraction of ice particles.~~ Future efforts should aim on calibration of the scattering pattern analysis thresholds and interpretation of the reported complexity to derive the complex fraction of ice particles. It would be useful to collect and analyse the particles offline with high resolution microscopy to confirm the airborne particle measurements. It should be highlighted that the phase of small spherical particles with low complexity cannot be unambiguously defined with any of these instruments and~~However,~~ the complexity of ice particles smaller than 7 µm remains unclear.

We have presented polarisation measurements of airborne and laboratory-instruments in an expansion chamber. We conclude that in these simulated atmospheric conditions the polarisation and depolarisation signal from frozen droplets have higher correlation at higher concentrations of small particles and can be comparable above certain concentration and size thresholds. These findings and the derived instrumental differences ~~can~~ may be used in the interpretation of atmospheric measurements of frozen droplets from remote and in situ combined campaigns as well as a pathway for further research and development of these instruments.

5 Appendix A

Figure A1 presents the temperature profile of the complementary adiabatic expansions at –40 and –50 °C. The resulting supersaturated conditions are annotated on the right y axis. The time series of small scale complexity at –40 and –50 °C segregated by size are shown in Fig. A2. Higher k-values are observed at lower temperature.

Acknowledgments. We would like to thank CERN for supporting CLOUD with important technical and financial resources. We express great appreciation for the CLOUD collaboration. This research has received funding from the EC Seventh Framework Programme (Marie Curie Initial Training Network "CLOUD-TRAIN" no. 316662). The SIMONE measurements were funded by the CERN CLOUD project. The PPD-2K instrument was fully funded by the Deutsche Forschungsgemeinschaft within project SCHN 1140/2-1. The CAPS and 3V-CPI instruments used in this work were supplied by the UK National Centre for Atmospheric Science.

References

Abdelmonem, A., Järvinen, E., Duft, D., Hirst, E., Vogt, S., Leisner, T., and Schnaiter, M.: PHIPS-HALO: The airborne Particle Habit Imaging and Polar Scattering probe. Part I: Design and Operation, Atmos. Meas. Tech. Discuss., doi:10.5194/amt-2016-42, in review, 2016.

Ackerman, A. S., Fridlind, A. M., Grandin, A., Dezitter, F., Weber, M., Strapp, J. W., and Korolev, A. V.: High ice water content at low radar reflectivity near deep convection – Part 2: Evaluation of microphysical pathways in updraft parcel simulations, Atmos. Chem. Phys., 15, 11729-11751, doi:10.5194/acp-15-11729-2015, 2015.

Baumgardner, D., Jonsson, H., Dawson, W., O'Connor, D., and Newton, R.: The cloud, aerosol and precipitation spectrometer: a new instrument for cloud investigations, Atmospheric Research, 59, 251-264, doi: 10.1016/S0169-8095(01)00119-3, 2001.

Baumgardner, D., Newton, R., Krämer, M., Meyer, J., Beyer, A., Wendisch, M., and Vochezer, P.: The Cloud Particle Spectrometer with Polarization Detection (CPSPD): A next generation open-path cloud probe for distinguishing liquid cloud droplets from ice crystals, Atmospheric Research, 142, 2-14, http://dx.doi.org/10.1016/j.atmosres.2013.12.010, 2014.

Borrmann, S., Luo, B., and Mishchenko, M.: Application of the T-matrix method to the measurement of aspherical (ellipsoidal) particles with forward scattering optical particle counters, J. Aerosol Sci., 31, 789–799, doi:10.1016/S0021-8502(99)00563-7, 2000.

Buck, Buck Research CR-1A User's Manual, Appendix 1, 1996.

Burton, S. P., Ferrare, R. A., Hostetler, C. A., Hair, J. W., Rogers, R. R., Obland, M. D., Butler, C. F., Cook, A. L., Harper, D. B., and Froyd, K. D.: Aerosol classification using airborne High Spectral Resolution Lidar measurements – methodology and examples, Atmos. Meas. Tech., 5, 73-98, doi: 10.5194/amt-5-73-2012, 2012.

Byers, H. R., and Braham, R. R.: Thunderstorm structure and circulation, J. Meteor., 5, 71-86, doi: 10.1175/1520-0469(1948)005<0071:TSAC>2.0.CO;2, 1948.

Cober, S. G., Isaac, G. A., Korolev, A. V., and Strapp, J. W.: Assessing Cloud-Phase Conditions, Journal of Applied Meteorology, 40, 1967-1983, doi:10.1175/1520-0450(2001)040<1967:ACPC>2.0.CO;2, 2001.

Connolly, P. J., Flynn, M. J., Ulanowski, Z., Choularton, T. W., Gallagher, M. W., and Bower, K. N.: Calibration of the Cloud Particle Imager Probes Using Calibration Beads and Ice Crystal Analogs: The Depth of Field, Journal of Atmospheric and Oceanic Technology, 24, 1860-1879, doi: 10.1175/JTECH2096.1, 2007.

Cotton, R., Osborne, S., Ulanowski, Z., Hirst, E., Kaye, P. H., and Greenaway, R. S.: The Ability of the Small Ice Detector (SID-2) to Characterize Cloud Particle and Aerosol Morphologies Obtained during Flights of the FAAM BAe-146 Research Aircraft, Journal of Atmospheric and Oceanic Technology, 27, 290-303, doi: 10.1175/2009JTECHA1282.1, 2010.

Dias, A., Ehrhart, S., Vogel, A., Williamson, C., Simões, J., Kirkby, J., Mathot, S., and Onnela, A.: Analysis of temperature homogeneity of the CLOUD chamber at CERN, in preparation, 2016

Droplet Measurement Technologies Manual: CAPS operator manual, DOC-0066 Revision F, DMT, Boulder, Colorado, USA, 2011.

Duplissy, J., Merikanto, J., Franchin, A., Tsagkogeorgas, G., Kangasluoma, J., Wimmer, D., Vuollekoski, H., Schobesberger, S., Lehtipalo, K., Flagan, R., Brus, D., Donahue, N., Vehkämäki, H., Almeida, J., Amorim, A., Barmet, P., Bianchi, F., Breitenlechner, M., Dunne, E., Guida, R., Henschel, H., Junninen, H., Kirkby, J., Kürten, A., Kupc, A., Määttänen, A., Makhmutov, V., Mathot, S., Nieminen, T., Onnela, A., Praplan, A.,

Riccobono, F., Rondo, L., Steiner, G., Tome, A., Walther, H., Baltensperger, U., Carslaw, K., Dommen, J., Hansel, A., Petäjä, T., Sipilä,M., Stratmann, F., Vrtala, A.,Wagner, P.,Worsnop, D., Curtius, J., and Kulmala,M.: Effect of ions on sulfuric acid-water binary particle formation II: Experimental data and comparison with QC-normalized classical nucleation theory, Journal of Geophysical Research: Atmospheres, doi:10.1002/2015JD023539, 2016.

Elliott, J. W., and Smith, F. T.: Ice formation on a smooth or rough cold surface due to the impact of a supercooled water droplet, Journal of Engineering Mathematics, 1-30, doi:10.1007/s10665-015-9784-z, 2015.

Emersic, C., Connolly, P. J., Boult, S., Campana, M., and Li, Z.: Investigating the discrepancy between wet-suspension- and dry-dispersion-derived ice nucleation efficiency of mineral particles, Atmos. Chem. Phys., 15, 11311-11326, doi: 10.5194/acp-15-11311-2015, 2015.

Gallagher, M.W, Baumgardner, D., Lloyd, G., Beswick, K., Freer, M., and Durant, A.: Detection and Analysis of High Ice Concentration Events and Supercooled Drizzle from IAGOS Commercial Aircraft, Geophys. Res. Abstr. Vol. 18, EGU2016-2924, EGU General Assembly, Vienna, Austria, 2016.

Garrett, T. J., Navarro, B. C., Twohy, C. H., Jensen, E. J., Baumgardner, D. G., Bui, P. T., Gerber, H., Herman, R. L., Heymsfield, A. J., Lawson, P., Minnis, P., Nguyen, L., Poellot, M., Pope, S. K., Valero, F. P. J., and Weinstock, E. M.: Evolution of a Florida Cirrus Anvil, J. Atmos. Sci., 62, 2352–2372, 2005.

Gayet, J.-F., Mioche, G., Shcherbakov, V., Gourbeyre, C., Busen, R., and Minikin, A.: Optical properties of pristine ice crystals in mid-latitude cirrus clouds: a case study during CIRCLE-2 experiment, Atmos. Chem. Phys., 11, 2537-2544, doi:10.5194/acp-11-2537-2011, 2011.

Gayet, J. F., Mioche, G., Bugliaro, L., Protat, A., Minikin, A., Wirth, M., Dörnbrack, A., Shcherbakov, V., Mayer, B., Garnier, A., and Gourbeyre, C.: On the observation of unusual high concentration of small chain-like aggregate ice crystals and large ice water contents near the top of a deep convective cloud during the CIRCLE-2 experiment, Atmos. Chem. Phys., 12, 727-744, doi:10.5194/acp-12-727-2012, 2012.

Glen, A. and Brooks, S. D.: A new method for measuring optical scattering properties of atmospherically relevant dusts using the Cloud and Aerosol Spectrometer with Polarization (CASPOL), Atmos. Chem. Phys., 13, 1345–1356, doi:10.5194/acp-13-1345-2013, 2013.

Guida, R., Carrie, P., De Menezes, L., Duplissy, J., Fayet, F., Kirkby, J., Mathot, S., Minginette, P., Onnela, A., Rochez, J., Thomas, G., Wasem, A., and Wilhelmsson, M.: An ultra-pure gas system for the CLOUD experiment at CERN, in: 2012 IEEE Nuclear Science Symposium and Medical Imaging Conference (NSS/MIC), 27 October–3 November 2012, Anaheim, CA, 1199–1203, 2012.

Guida, R., Carrie, P., De Menezes, L., Duplissy, J., Fayet, F., Haider, S., Kirkby, J., Mathot, S., Minginette, P., Onnela, A., Rochez, J., Thomas, G., Wasem, A., and Wilhelmsson, M.: Development of the gas system for the CLOUD experiment at CERN, in: Nuclear Science Symposium and Medical Imaging Conference (NSS/MIC), 2013 IEEE, Seoul 27 October–2 November 2013, 1–5, 2013.

Heymsfield, A. J., Miloshevich, L. M., Schmitt, C., Bansemer, A., Twohy, C., Poellot, M. R., Fridlind, A., and Gerber, H.: Homogeneous Ice Nucleation in Subtropical and Tropical Convection and Its Influence on Cirrus Anvil Microphysics, J. Atmos. Sci., 62, 41-64, doi:10.1175/JAS-3360.1, 2005.

~~Heymsfield, A. J., Schmitt, C., Bansemer, A., and Twohy, C. H.: Improved Representation of Ice Particle Masses Based on Observations in Natural Clouds, Journal of the Atmospheric Sciences, 67, 3303-3318, doi:10.1175/2010JAS3507.1, 2010.~~

Hirst, E., Kaye, P. H., Greenaway, R. S., Field, P., and Johnson, D. W.: Discrimination of micrometre-sized ice and super-cooled droplets in mixed-phase cloud, Atmospheric Environment, 35, 33-47, http://dx.doi.org/10.1016/S1352-2310(00)00377-0, 2001.

Irvine, E. A. and Shine, K. P.: Ice supersaturation and the potential for contrail formation in a changing climate, Earth Syst. Dynam., 6, 555-568, doi: 10.5194/esd-6-555-2015, 2015.

Järvinen, E., Ignatius, K., Nichman, L., Kristensen, T. B., Fuchs, C., Hoyle, C. R., Höppel, N., Corbin, J. C., Craven, J., Duplissy, J., Ehrhart, S., El Haddad, I., Frege, C., Gordon, H., Jokinen, T., Kallinger, P., Kirkby, J., Kiselev, A., Naumann, K.-H., Petäjä, T., Pinterich, T., Prevot, A. S. H., Saathoff, H., Schiebel, T., Sengupta, K., Simon, M., Slowik, J. G., Tröstl, J., Virtanen, A., Vochezer, P., Vogt, S., Wagner, A. C., Wagner, R., Williamson, C., Winkler, P. M., Yan, C., Baltensperger, U., Donahue, N. M., Flagan, R. C., Gallagher, M., Hansel, A., Kulmala, M., Stratmann, F., Worsnop, D. R., Möhler, O., Leisner, T., and Schnaiter, M.: Observation of viscosity transition in α-pinene secondary organic aerosol, Atmos. Chem. Phys., 16, 4423-4438, doi:10.5194/acp-16-4423-2016, 2016a.

Järvinen, E., Kemppinen, O., Nousiainen, T., Kociok, T., Möhler, O., Leisner, T., and Schnaiter, M.: Laboratory investigations of mineral dust near-backscattering depolarization ratios, Journal of Quantitative Spectroscopy and Radiative Transfer, 178, 192-208, http://dx.doi.org/10.1016/j.jqsrt.2016.02.003, 2016b.

Järvinen, E., Schnaiter, M., Mioche, G., Jourdan, O., Shcherbakov, V. N., Costa, A., Afchine, A., Krämer, M., Heidelberg, F., Jurkat, T., Voigt, C., Schlager, H., Nichman, L., Gallagher, M., Hirst, E., Schmitt, C., Bansemer, A., Heymsfield, A., Lawson, P., Tricoli, U., Pfeilsticker, K., Vochezer, P., Möhler, O., and Leisner, T.: Quasi-Spherical Ice in Convective Clouds, Journal of the Atmospheric Sciences, 73, 3885-3910, doi:10.1175/JAS-D-15-0365.1, 2016c.

Jeanne, M., Walter, S., and Philip, C.: The Ice Particle Threat to Engines in Flight, in: 44th AIAA Aerospace Sciences Meeting and Exhibit, Aerospace Sciences Meetings, American Institute of Aeronautics and Astronautics, 2006.

Jensen, E. J., Lawson, P., Baker, B., Pilson, B., Mo, Q., Heymsfield, A. J., Bansemer, A., Bui, T. P., McGill, M., Hlavka, D., Heymsfield, G., Platnick, S., Arnold, G. T., and Tanelli, S.: On the importance of small ice crystals in tropical anvil cirrus, Atmos. Chem. Phys., 9, 5519-5537, doi: 10.5194/acp-9-5519-2009, 2009.

Jensen, E., Pfister, L., Bui, T.-P., Lawson, P., and Baumgardner, D.: Ice nucleation and cloud microphysical properties in tropical tropopause layer cirrus, Atmos. Chem. Phys., 10, 1369-1384, 2010.

Johnson, A., Lasher-Trapp, S., Bansemer, A., Ulanowski, Z., and Heymsfield, A. J.: Difficulties in Early Ice Detection with the Small Ice Detector-2 HIAPER (SID-2H) in Maritime Cumuli, Journal of Atmospheric and Oceanic Technology, 31, 1263-1275, doi: 10.1175/JTECH-D-13-00079.1, 2014.

Johnson, B., Turnbull, K., Brown, P., Burgess, R., Dorsey, J., Baran, A. J., Webster, H., Haywood, J., Cotton, R., Ulanowski, Z., Hesse, E., Woolley, A., and Rosenberg, P.: In situ observations of volcanic ash clouds from the FAAM aircraft during the eruption of Eyjafjallajökull in 2010, Journal of Geophysical Research: Atmospheres, 117, D00U24, doi: 10.1029/2011JD016760, 2012.

Kirkby, J., Curtius, J., Almeida, J., Dunne, E., Duplissy, J., Ehrhart, S., Franchin, A., Gagne, S., Ickes, L., Kürten, A., Kupc, A., Metzger, A., Riccobono, F., Rondo, L., Schobesberger, S., Tsagkogeorgas, G., Wimmer, D., Amorim, A., Bianchi, F., Breitenlechner, M., David, A., Dommen, J., Downard, A., Ehn, M., Flagan, R. C., Haider, S., Hansel, A., Hauser, D., Jud, W., Junninen, H., Kreissl, F., Kvashin, A., Laaksonen, A., Lehtipalo, K.,

Lima, J., Lovejoy, E. R., Makhmutov, V., Mathot, S., Mikkilä, J., Minginette, P., Mogo, S., Nieminen, T., Onnela, A., Pereira, P., Petäjä, T., Schnitzhofer, R., Seinfeld, J. H., Sipilä, M., Stozhkov, Y., Stratmann, F., Tomé, A., Vanhanen, J., Viisanen, Y., Vrtala, A., Wagner, P. E., Walther, H., Weingartner, E., Wex, H., Winkler, P. M., Carslaw, K. E., Worsnop, D. R., Baltensperger, U., and Kulmala, M.: Role of sulphuric acid, ammonia and galactic cosmic rays in atmospheric aerosol nucleation, Nature, 476, 429–433, 2011.

Korolev, A., and Isaac, G.: Phase transformation of mixed-phase clouds, Q. J. R. Meteorol. Soc., 129, 19-38, doi: 10.1256/qj.01.203, 2003a.

Korolev, A., and Isaac, G.: Roundness and Aspect Ratio of Particles in Ice Clouds, J. Atmos. Sci., 60, 1795-1808, doi: 10.1175/1520-0469(2003)060<1795:RAAROP>2.0.CO;2, 2003b.

Korolev, A. V., Isaac, G. A., Cober, S. G., Strapp, J. W., and Hallett, J.: Microphysical characterization of mixed-phase clouds, Q. J. R. Meteorol. Soc., 129, 39-65, 10.1256/qj.01.204, 2003c.

Krämer, M., Rolf, C., Luebke, A., Afchine, A., Spelten, N., Costa, A., Meyer, J., Zöger, M., Smith, J., Herman, R. L., Buchholz, B., Ebert, V., Baumgardner, D., Borrmann, S., Klingebiel, M., and Avallone, L.: A microphysics guide to cirrus clouds – Part 1: Cirrus types, Atmos. Chem. Phys., 16, 3463-3483, doi:10.5194/acp-16-3463-2016, 2016.

Lance, S.: Coincidence Errors in a Cloud Droplet Probe (CDP) and a Cloud and Aerosol Spectrometer (CAS), and the Improved Performance of a Modified CDP, Journal of Atmospheric and Oceanic Technology, 29, 1532-1541, doi:10.1175/JTECH-D-11-00208.1, 2012.

Lawson, R. P., Heymsfield, A. J., Aulenbach, S. M., and Jensen, T. L.: Shapes, sizes and light scattering properties of ice crystals in cirrus and a persistent contrail during SUCCESS, Geophysical Research Letters, 25, 1331-1334, doi: 10.1029/98GL00241, 1998.

Lawson, R. P., Baker, B.A., Schmitt, C.G., and Jensen, T.L.: An overview of microphysical properties of Arctic clouds observed in May and July during FIRE ACE. J. Geophys. Res., 106, 14 989–15 014, 2001.

Lawson, R. P., Baker, B., Pilson, B., and Mo, Q.: In Situ Observations of the Microphysical Properties of Wave, Cirrus, and Anvil Clouds. Part II: Cirrus Clouds, J. Atmos. Sci., 63, 3186-3203, doi:10.1175/JAS3803.1, 2006a.

Lawson, R. P., Baker, B. A., Zmarzly, P., O'Connor, D., Mo, Q., Gayet, J.-F., and Shcherbakov, V.: Microphysical and Optical Properties of Atmospheric Ice Crystals at South Pole Station, Journal of Applied Meteorology and Climatology, 45, 1505-1524, doi:10.1175/JAM2421.1, 2006b.

Lawson, R. P., O'Connor, D., Zmarzly, P., Weaver, K., Baker, B., Mo, Q., and Jonsson, H.: The 2D-S (Stereo) Probe: Design and Preliminary Tests of a New Airborne, High-Speed, High-Resolution Particle Imaging Probe, Journal of Atmospheric and Oceanic Technology, 23, 1462-1477, doi:10.1175/JTECH1927.1, ~~2006b~~2006c.

Luebke, A. E., Afchine, A., Costa, A., Grooß, J.-U., Meyer, J., Rolf, C., Spelten, N., Avallone, L. M., Baumgardner, D., and Krämer, M.: The origin of midlatitude ice clouds and the resulting influence on their microphysical properties, Atmos. Chem. Phys., 16, 5793-5809, doi:10.5194/acp-16-5793-2016, 2016.

Lynch, D. K.: Cirrus, Oxford University Press, 2001.

Möhler, O., Field, P. R., Connolly, P., Benz, S., Saathoff, H., Schnaiter, M., Wagner, R., Cotton, R., Krämer, M., Mangold, A., and Heymsfield, A. J.: Efficiency of the deposition mode ice nucleation on mineral dust particles, Atmos. Chem. Phys., 6, 3007–3021, doi:10.5194/acp-6-3007-2006, 2006.

Nelson, J.: Sublimation of Ice Crystals. J. Atmos. Sci. 55, 910-919 (1998).

Nichman, L., Fuchs, C., Järvinen, E., Ignatius, K., Höppel, N. F., Dias, A., Heinritzi, M., Simon, M., Tröstl, J., Wagner, A. C., Wagner, R., Williamson, C., Yan, C., Connolly, P. J., Dorsey, J. R., Duplissy, J., Ehrhart, S., Frege, C., Gordon, H., Hoyle, C. R., Kristensen, T. B., Steiner, G., McPherson Donahue, N., Flagan, R., Gallagher, M. W., Kirkby, J., Möhler, O., Saathoff, H., Schnaiter, M., Stratmann, F., and Tomé, A.: Phase transition observations and discrimination of small cloud particles by light polarization in expansion chamber experiments, Atmos. Chem. Phys., 16, 3651-3664, doi:10.5194/acp-16-3651-2016, 2016.

Petzold, A., Esselborn, M., Weinzierl, B., Ehret, G., Ansmann, A., Müller, D., Donovan, D., van Zadelhoff, G.-J., Berthier, S., Wiegner, M., Gasteiger, J., Buras, R., Mayer, B., Lajas, D., and Wehr, T.: ICAROHS inter-comparison of aerosol retrievals and observational requirements for multi-wavelength HSRL systems, in: Proceedings of the ESA Living Planet Symposium, Bergen, Norway, ESA SP-686, December 2010, edited by: Lacoste-Francis, H., ESA Communications published and distributed by: ESA Communications, ESTEC, Noordwijk, the Netherlands, p. 102, 2010.

Rosenfeld, D., and Woodley, W. L.: Deep convective clouds with sustained supercooled liquid water down to -37.5 °C, Nature, 405, 440-442, 2000.

Sachweh, B., Barthel, H., Polke, R., Umhauer, H., and Büttner, H.: Particle shape and structure analysis from the spatial intensity pattern of scattered light using different measuring devices, J. Aerosol Sci., 30, 1257-1270, http://dx.doi.org/10.1016/S0021-8502(99)00045-2, 1999.

Schnaiter, M., Büttner, S., Möhler, O., Skrotzki, J., Vragel, M., and Wagner, R.: Influence of particle size and shape on the backscattering linear depolarisation ratio of small ice crystals – cloud chamber measurements in the context of contrail and cirrus microphysics, Atmos. Chem. Phys., 12, 10465–10484, doi:10.5194/acp-12-10465-2012, 2012.

Schnaiter, M., Järvinen, E., Vochezer, P., Abdelmonem, A., Wagner, R., Jourdan, O., Mioche, G., Shcherbakov, V. N., Schmitt, C. G., Tricoli, U., Ulanowski, Z., and Heymsfield, A. J.: Cloud chamber experiments on the origin of ice crystal complexity in cirrus clouds, Atmos. Chem. Phys., 16, 5091-5110, doi:10.5194/acp-16-5091-2016, 2016.

Stith, J. L., Avallone, L. M., Bansemer, A., Basarab, B., Dorsi, S. W., Fuchs, B., Lawson, R. P., Rogers, D. C., Rutledge, S., and Toohey, D. W.: Ice particles in the upper anvil regions of midlatitude continental thunderstorms: the case for frozen-drop aggregates, Atmos. Chem. Phys., 14, 1973-1985, doi:10.5194/acp-14-1973-2014, 2014.

Stordal, F., Myhre, G., Stordal, E. J. G., Rossow, W. B., Lee, D. S., Arlander, D. W., and Svendby, T.: Is there a trend in cirrus cloud cover due to aircraft traffic?, Atmos. Chem. Phys., 5, 2155-2162, doi:10.5194/acp-5-2155-2005, 2005.

Taylor, J. W., Choularton, T. W., Blyth, A. M., Liu, Z., Bower, K. N., Crosier, J., Gallagher, M. W., Williams, P. I., Dorsey, J. R., Flynn, M. J., Bennett, L. J., Huang, Y., French, J., Korolev, A., and Brown, P. R. A.: Observations of cloud microphysics and ice formation during COPE, Atmos. Chem. Phys., 16, 799-826, doi:10.5194/acp-16-799-2016, 2016.

Vochezer, P., Järvinen, E., Wagner, R., Kupiszewski, P., Leisner, T., and Schnaiter, M.: In situ characterization of mixed phase clouds using the Small Ice Detector and the Particle Phase Discriminator, Atmos. Meas. Tech., 9, 159-177, doi: 10.5194/amt-9-159-2016, 2016.

Wagner, R., Benz, S., Bunz, H., Möhler, O., Saathoff, H., Schnaiter, M., Leisner, T., and Ebert, V.: Infrared optical constants of highly diluted sulfuric acid solution droplets at cirrus temperatures, J. Phys. Chem. A, 112, 11661–11676, 2008.

Wallace, J. M., and Hobbs, P. V.: 6 - Cloud Microphysics, in: Atmospheric Science (Second Edition), Academic Press, San Diego, 209-269, 2006.

Wendisch, M., and Brenguier, J.-L.: Airborne Measurements for Environmental Research: Methods and Instruments, John Wiley & Sons, 2013.

Zhang, C., and Harrington, J. Y.: The Effects of Surface Kinetics on Crystal Growth and Homogeneous Freezing in Parcel Simulations of Cirrus, J. Atmos. Sci., 72, 2929-2946, doi: 10.1175/JAS-D-14-0285.1, 2015.

Table 1: List of experiments. CCN concentration measured with CPC at the beginning of each expansion. Cloud particle dN/dlogD_p (water and ice) for the mean diameter is shown in the last column.

Exp. number	CCN conc. [cm^{-3}]	Cooling rate [°C min^{-1}]	T start [°C]	Mean diameter [µm]	~~Mean~~ dN/dlogD_p [cm^{-3}]
1276.05	220	–5	–40	7.9	48
1291.07	160	–5.8	–30	10	41.7
1291.12	110	–4.8	–30	15	30
1292.01	150	–4.9	–30	12	41.7
1298.12	110	–2.1	–50	9	6.5
1298.20	750	–3.1	–50	8	9.9

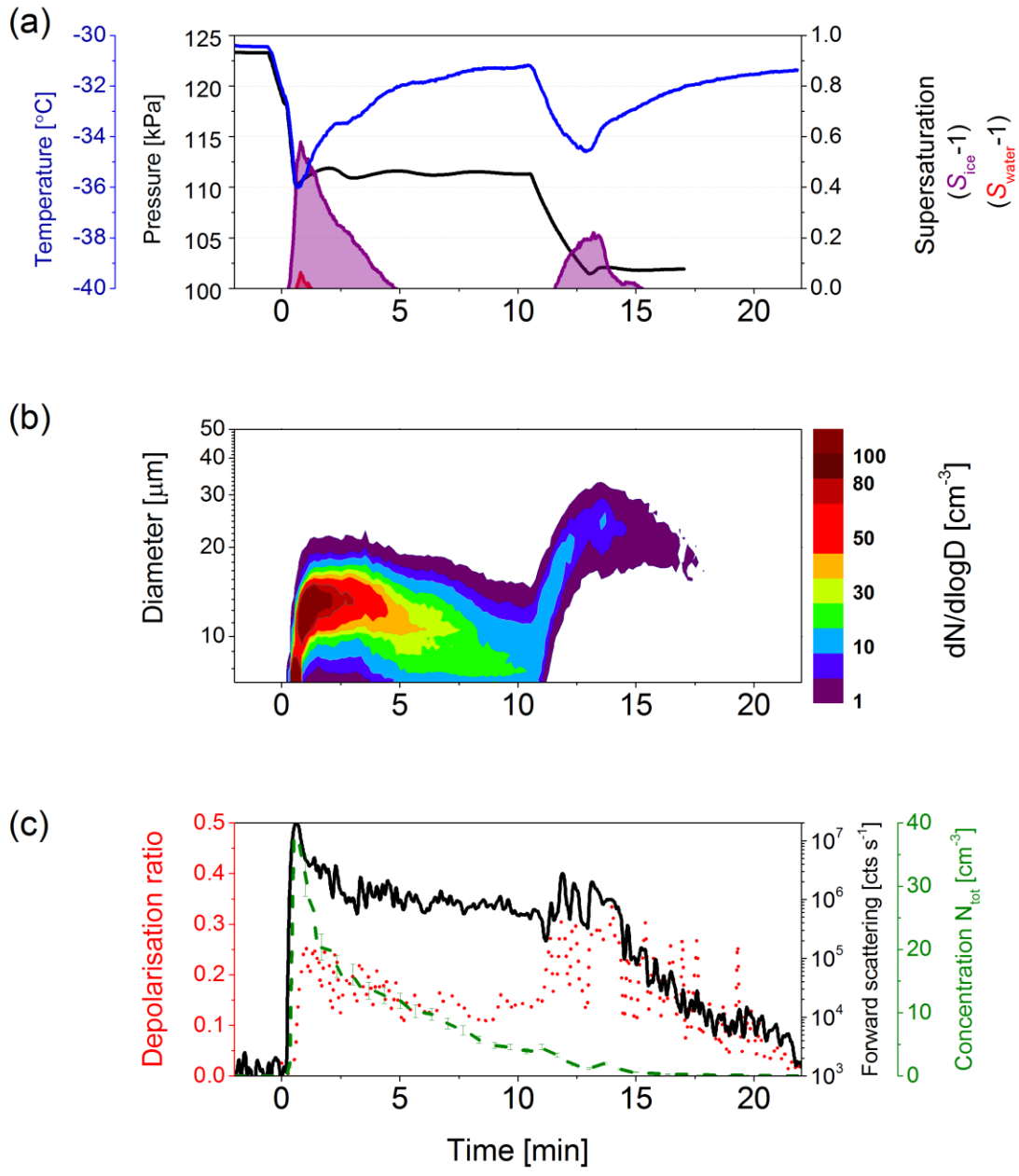

Figure 1. Homogeneous ice nucleation and regrowth experiment no. 1292.01 (–30 °C). (a) The development of pressure, temperature and supersaturation calculated from chilled mirror hygrometer (MBW373LX) and thermocouples measurements. Supersaturation with respect to ice is coloured in purple and with respect to water is coloured in red. Cloud forms at t=0 min, (b) The size distribution measured with PPD-2K, (c) SIMONE measurements of the forward scattering intensity (black solid line) and depolarisation ratio (red dotted line) together with the total number concentration measured by the PPD-2K (green dashed line).

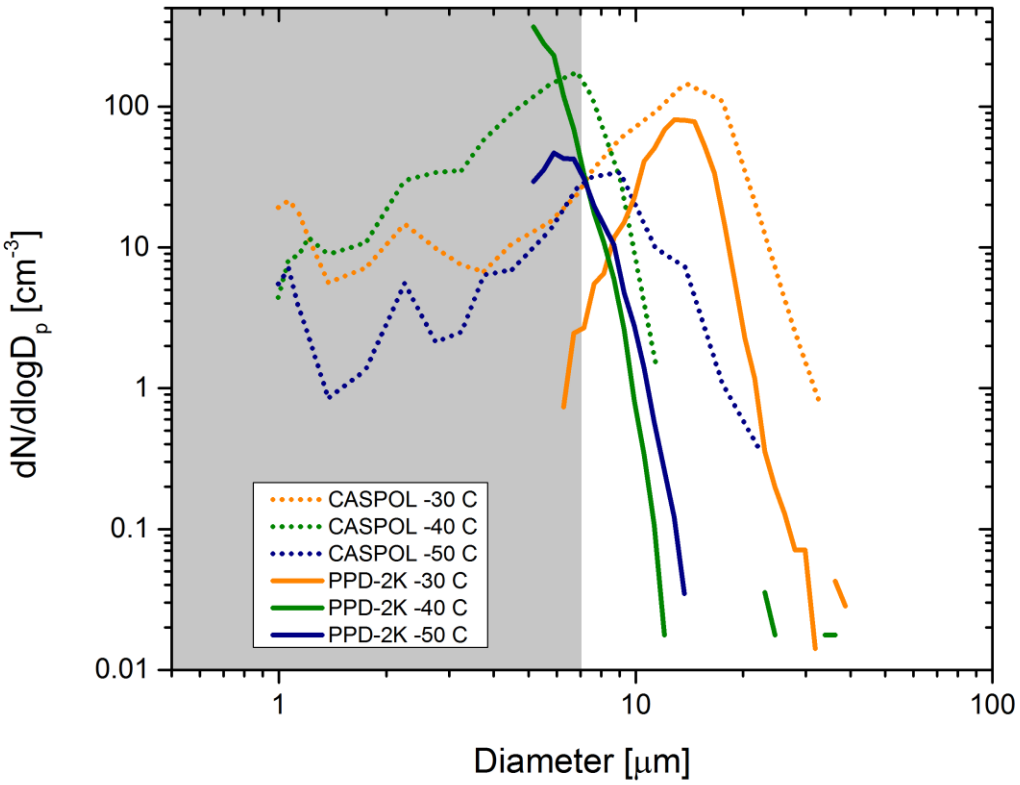

Figure 2. Selected 1 min averaged particle size distributions for runs: 1292.01 (–30 °C), 1276.05 (–40 °C), 1298.12 (–50 °C). White area represents the overlap in the size range of PPD-2K and CASPOL. Grey area represents the particles that are mostly present in the 292 PBP polarisation data points in a second. The aspherical fraction for comparison in Fig. 6 is derived from the white area.

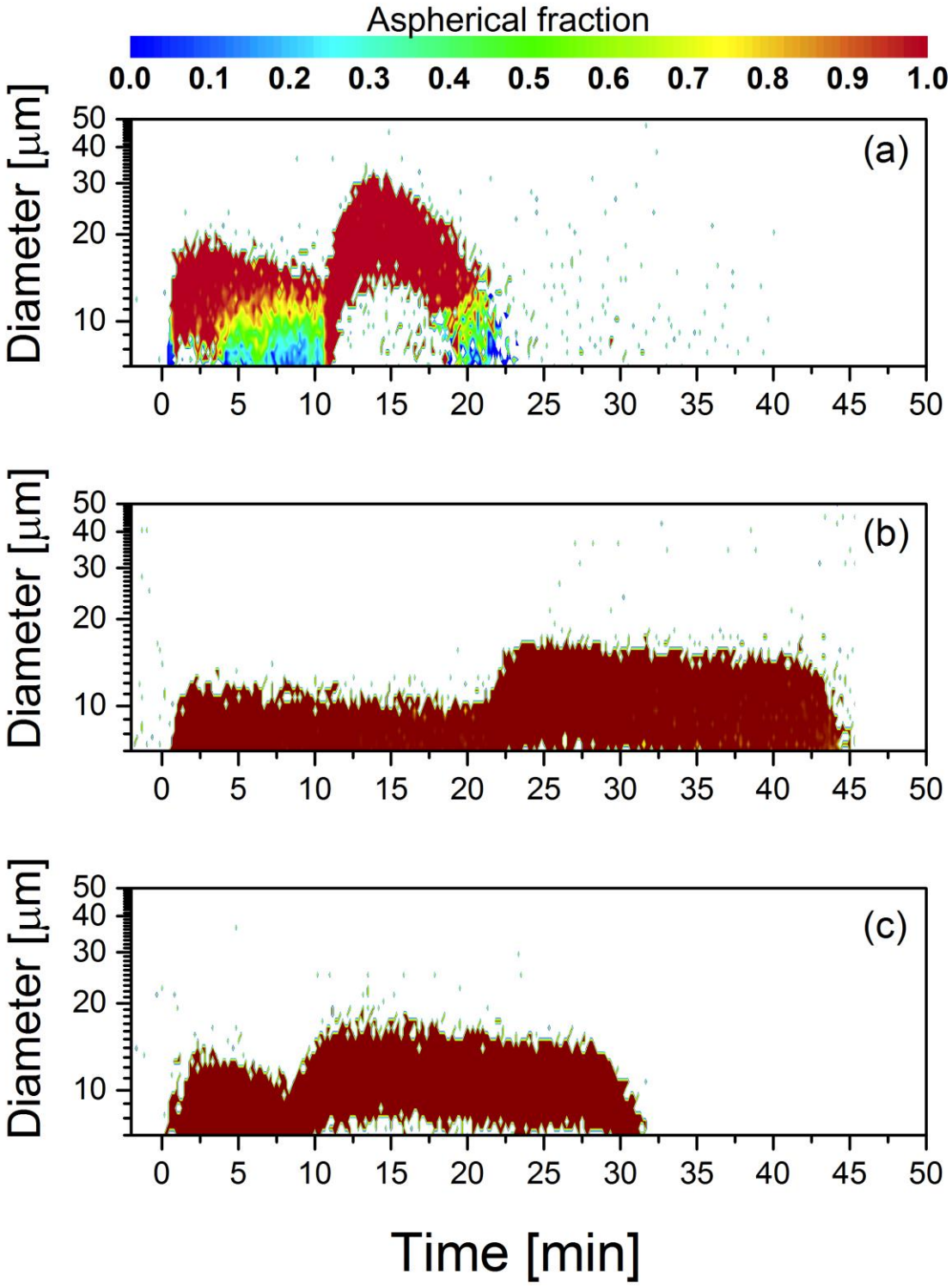

Figure 3. Size-segregated aspherical fraction measured by PPD-2K (see Sect. 2.3.1). (a) Run no. 1292.01 (–30 °C), (b) Run no. 1276.05 (–40 °C), (c) Run no. 1298.12 (–50 °C).

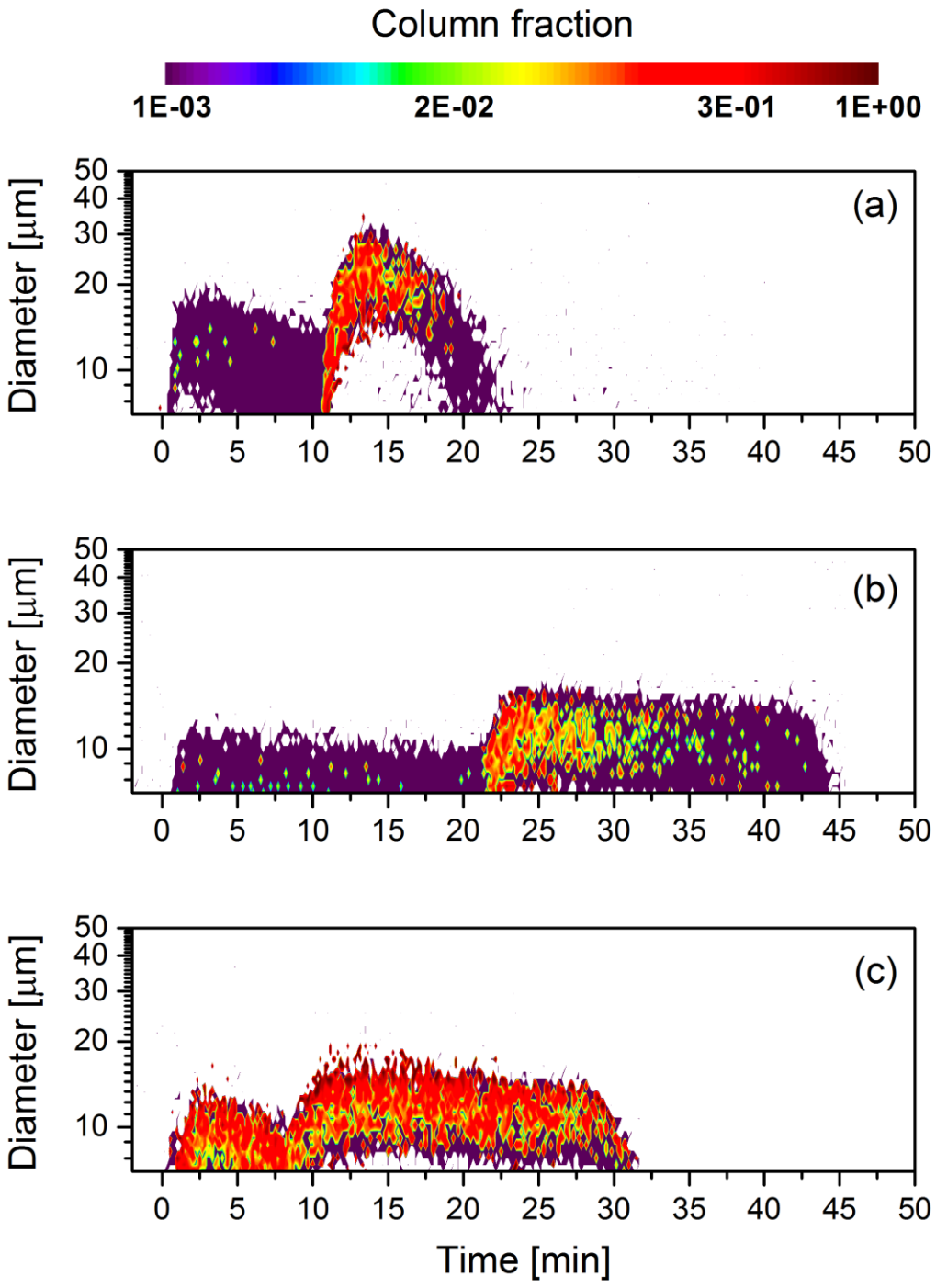

Figure 4. Size segregated fraction of columns on log scale, measured by PPD-2K. (a) Run no. 1292.01 (–30 °C), (b) Run no. 1276.05 (–40 °C), (c) Run no. 1298.12 (–50 °C).

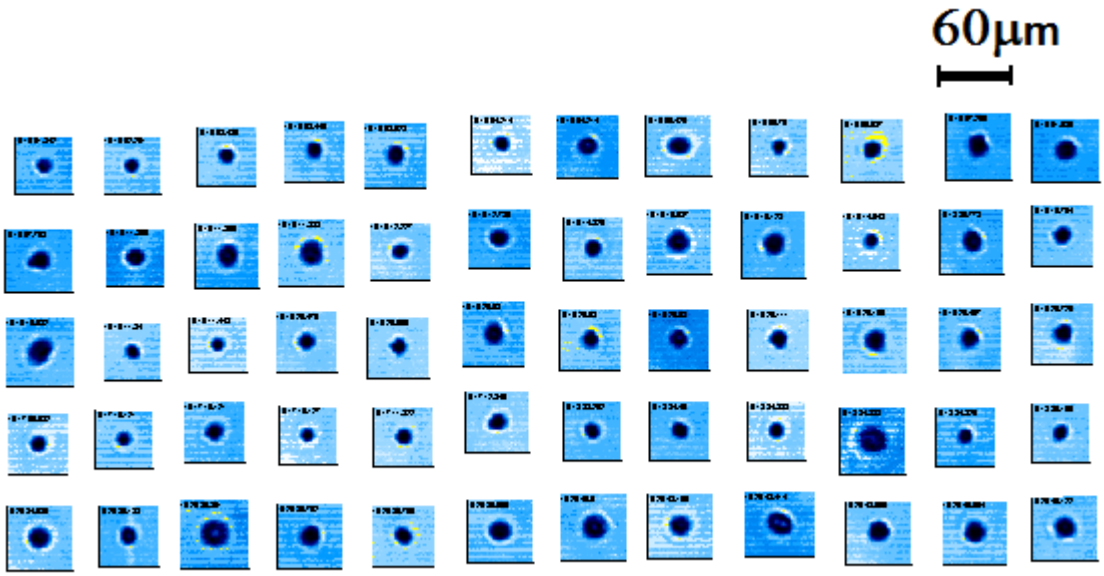

Figure 5. Experiment no. 1292.01. 3V-CPI images of frozen droplets immediately after phase transition. Shape analysis of these particles is presented in Fig.6.

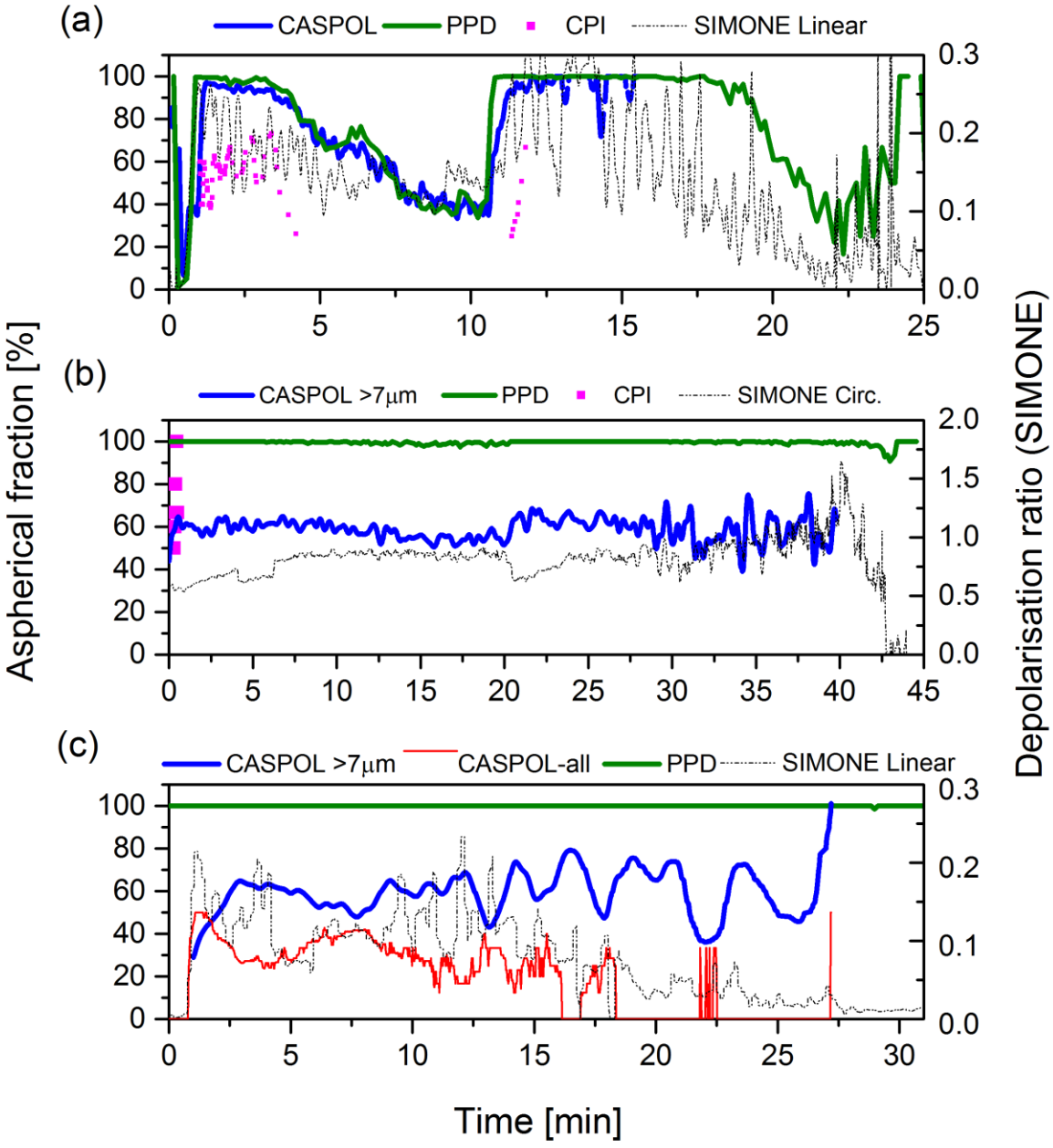

Figure 6. PPD-2K (green line), CASPOL (blue line) aspherical fraction of a subgroup of particles with diameter > 7 µm. The inter-comparison complemented by SIMONE linear or circular depolarisation ratio (dashed line), CASPOL aspherical fraction for all diameters (red line) and 3V- CPI non-round (aspherical) fraction (~~grey~~ magenta rectangles). (a) Run no. 1292.01 (–30 °C), (b) Run no. 1276.05 (–40 °C), (c) Run no. 1298.12 (–50 °C).

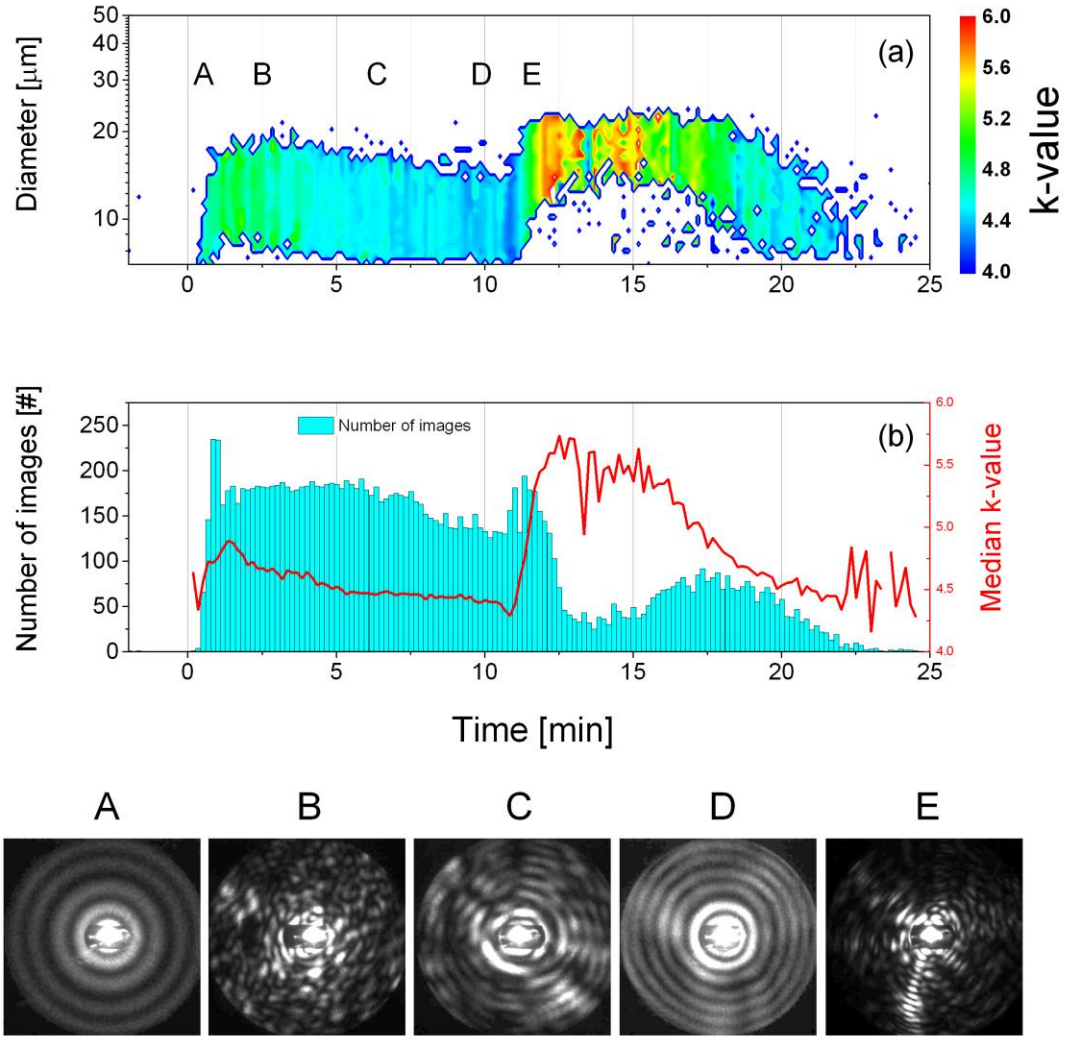

Figure 7. Evolution of small-scale complexity in experiment 1292.01 (–30 °C). (a) The size-segregated k-value (complexity parameter), capital letters correspond to the scattering patterns presented at the bottom, (b) Number of the scattering images used for the analysis and the median k-value. Lowest panel: 2-D scattering patterns from PPD-2K that have been collected during periods indicated with the letters A–E. For size segregated k-values at lower temperatures see Fig. A2~~S2~~.

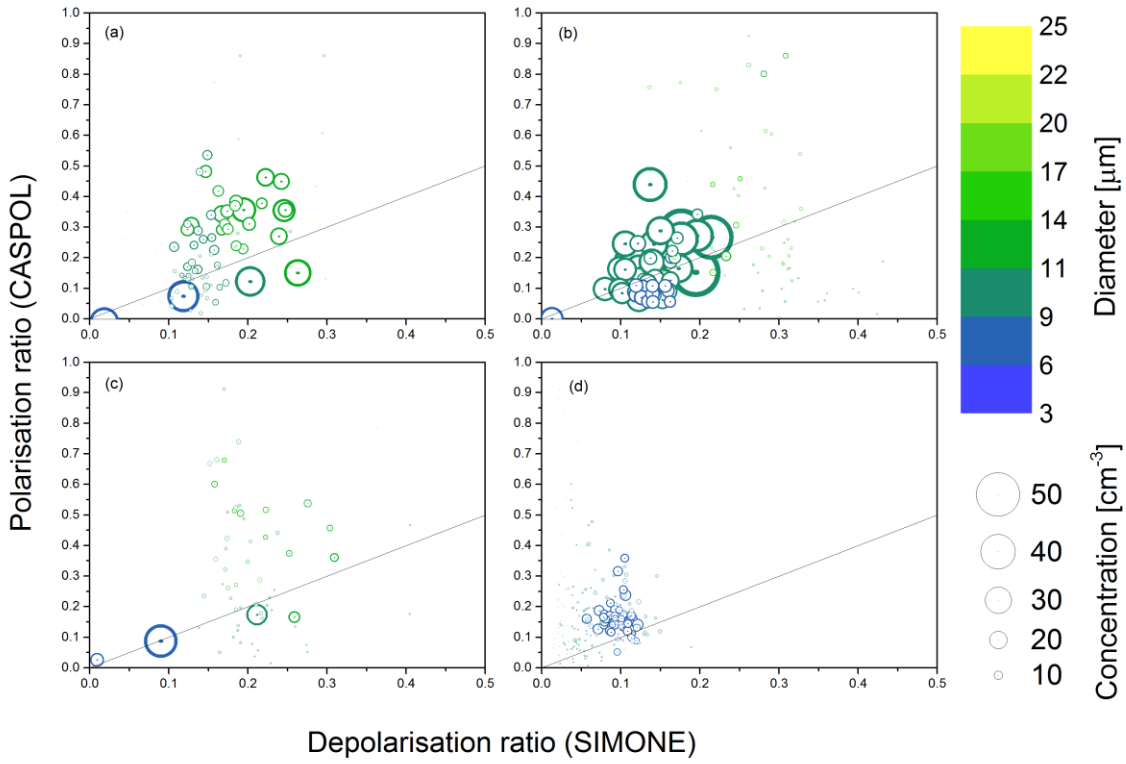

Figure 8. CASPOL polarisation and SIMONE depolarisation comparison for runs (a) no. 1292.01, (b) no. 1291.07, (c) no. 1291.12, (d) no. 1298.20, for details see Table 1. Marker size annotates number concentration, with highest at 56 cm^{-3}. Diameter is colour coded. Black reference line is 1:1 ratio. Better correlation is observed for clouds with higher concentration of small particles.

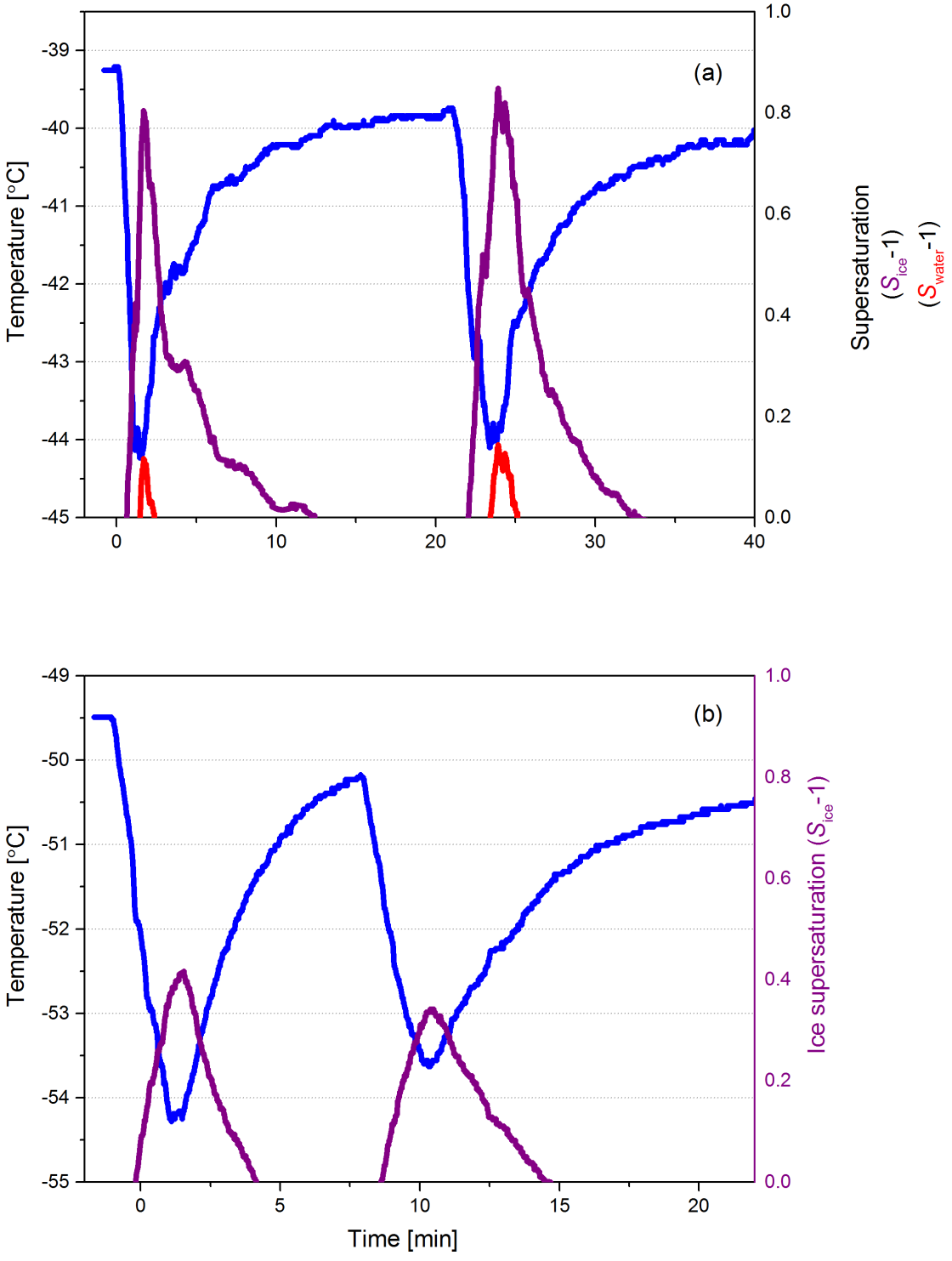

Figure A1. Temperature profiles and super-saturation. (a) Run no. 1276.05 (–40 °C), (b) Run no. 1298.12 (–50 °C).

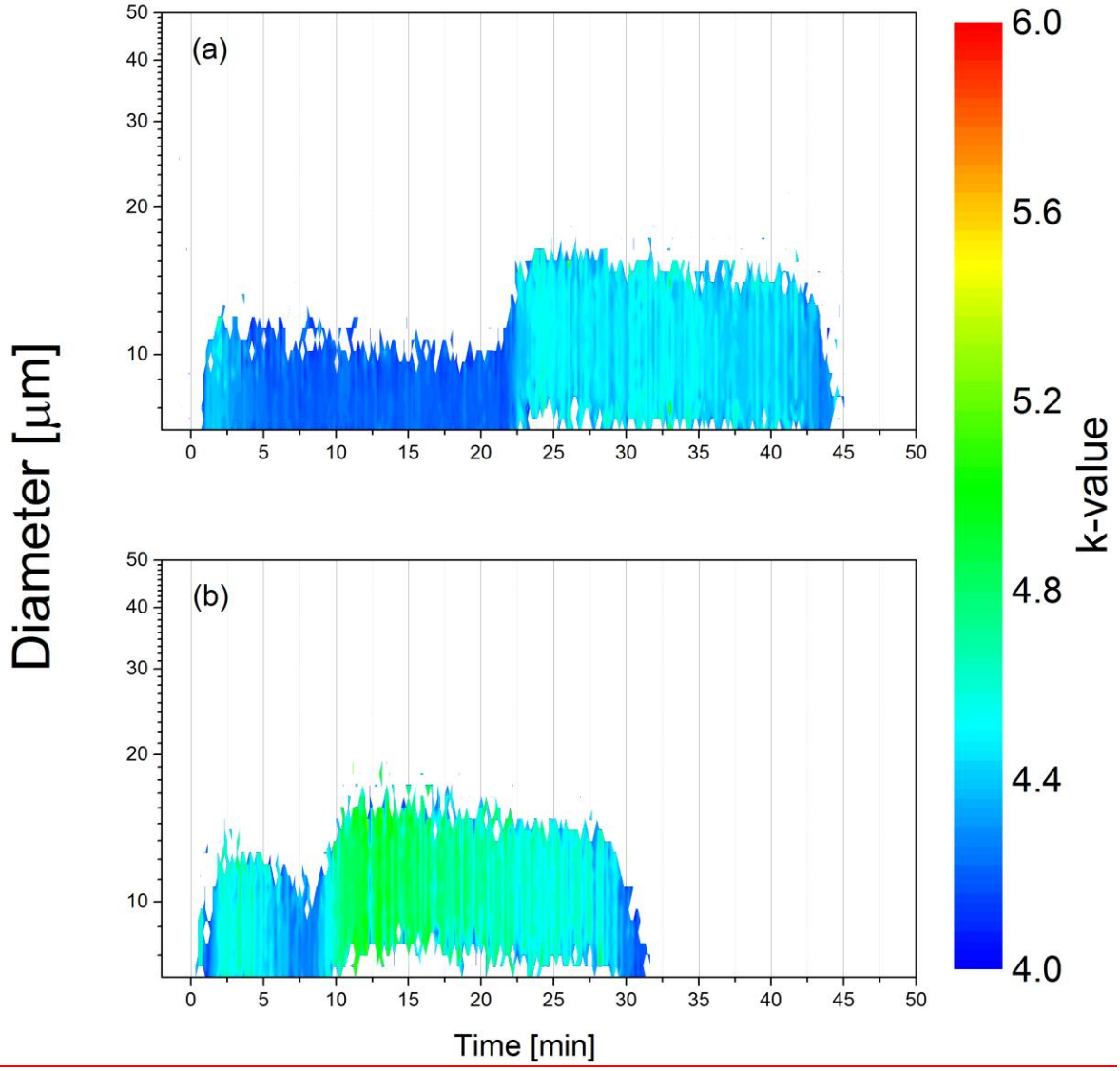

Figure A2. Evolution of small-scale complexity represented by the size-segregated k-value (complexity parameter (Schaniter et al., 2016)). (a) Run no. 1276.05 (–40 °C), (b) Run no. 1298.12 (–50 °C).